

MONITORING OF LANDSLIDE IN KANGWONDO AREA BY 2-PASS DIFFERENTIAL INTERFEROMETRY TECHNIQUE

Jung, Jae-Hoon

School of Civil & Environmental Engineering, Yonsei University, Korea
lionheart_kr@yonsei.ac.kr

KEY WORDS: Landslides, Change Detection, Disaster, SAR, correlation, interferometry

ABSTRACT:

Korea Peninsula is exposed to landslide problems because large regions of Korea are composed of mountain. As a result, we have a great loss of life and property every year. Conventional survey has many restrictions in terms of time and man power. In recent days, remote sensing has been utilized as an effective technique to detect damaged place as it has many advantages over conventional methods. Synthetic Aperture Radar (SAR) provides the all-weather capability and complements information available. Through differential interferometry technique, we can measure even very small displacement effect. In this study, we generated 12 interferograms of Kangwondo area from JERS-1 satellite images between 1992 and 1998, and monitored landslide area. As a result, around Auda mountain (N 37°. 50', E 128°. 37') and Gebang mountain (N 37°. 44', E 128°. 29') in the north part of Kangwondo and around Uljin(N 37°. 00', E 129°. 08') and Gagok(N 37°.08', E 129°.12') city which is located in the south part of Kangwondo are detected as damaged area by landslide. Also, comparing with weather forecast data, landslide in Korea is much affected with a heavy rain during the rainy spell in summer.

1. INTRODUCTION

In recent days, climatic changes cause abnormal weather all over the world and we have a great loss of life and property every year. In Korea, we suffer from landslide problem because large regions of Korea Peninsula are composed of mountain. Rapid detection and to take follow-up measures of disaster, the remote sensing is being used actively in many countries as conventional field survey has many restrictions in accessibility because of more time and man power requirement.

Synthetic Aperture Radar (SAR) is one of the techniques that has our attention. It is an active, imaging method using microwaves, which is carried on mobile platforms such as aeroplanes or satellites. Compared to passive methods deployed in the optical sensor that image an area by means of reflected sunlight, SAR allows unrestricted service irrespective of solar radiation and daytime. Moreover, it enables to choose the transmitted wave length in such a way that the attenuation of electromagnetic waves caused by the atmosphere can be disregarded(Achim, 2004). Thus the SAR sensor can be operated under almost any weather conditions and it enables us to detect disaster at anytime.

Gabriel and others first demonstrated the differential interferometry method in 1989. In this work, he measured the swelling of irrigated fields in Imperial Valley using SEASAT data. And few years later, Massonnet and others captured the centimetric deformation field of the Landers earthquake in 1992 by differential interferometry and published their study in *Nature*. Since then, differential interferometry has been applied to many researches such as detecting seismic events, volcanic deflation, ground subsidence, fluid pumping and landslide.

2. 2-PASS DINSAR TECHNIQUE

2.1 Fundamental theory

A conventional SAR only measures the location of a target in a two-dimensional coordinate system. However, the development of interferometric SAR (InSAR) technique has enabled us to measure the three dimension information(Rosen et al. 2000). The conventional antenna transmits the radar pulse and radar echoes from terrain are received by both the conventional and an additional antenna. Through combining the received signals from the two antennas, phase difference can be obtained. This phase difference contains the information about the angle from which the radar echo returned and can be converted into an altitude by combining with the distance information. The major difference between the SAR interferometry and stereoscopy is that InSAR technique uses the phase difference to obtain a topographic height of the image point.

In case two data are acquired in different time by two flights covering the same region, the interferometric measurement contains two kinds of phase information, terrain altitude and radial motion or displacement. We call it repeat-track interferometry and the basic idea of differential interferometric processing is to separate only displacement information from the total phase.

The amount of displacement can be acquired by removing the topography related phase. According to the methods subtracting this topography phase, there are three kinds of common methods in differential interferometry, 2-pass, 3-pass, and 4-pass. In case of 2-pass, the simulated topography phase is generated from a conventional DEM and 3-pass or 4-pass using an independent interferometric pair without phase component of topography change. 2-pass method has been developed by Massonnet and others, and became one of the most common methods in differential interferometry. In this study, we aimed to monitor the landslide by 2-Pass DInSAR technique.

2.2 Geometry of SAR interferometry

The interferometric phase is related with the discrepancy between two observations. If we consider the first observation is master and the second one is slave, and the distances between two antennas and target are ρ and $\rho + \delta\rho$, the interferometric phase can be defined by the baseline B and look angle θ . The geometry of the repeat-pass of SAR satellite is illustrated in Figure 1.

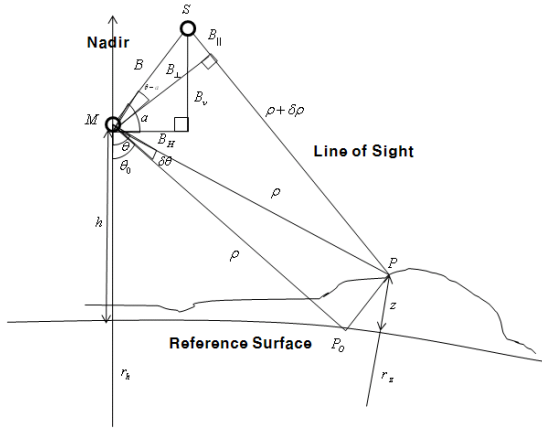


Figure 1. InSAR geometry

And the symbols of Figure 1 are defined as Table 1.

Symbol	Definition
M	Master antenna
B	Baseline
S	Slave antenna
$B_{ }$	Parallel baseline
z	Topographic height of target
B_{\perp}	Perpendicular baseline
h	Satellite height
B_v	Vertical baseline
r_h	Radius of earth at nadir
B_H	Horizontal baseline
r_z	Radius of earth at target
P	Target Position
P_0	Position on the reference surface same slant range as target P

Table 1. Definition of InSAR geometry symbols

From Figure 1, the phase difference between two antennas is given by the following E.q. (1).

$$\phi = \frac{4\pi}{\lambda} \delta\rho \quad (1)$$

Where λ is the wave length of sensor. $\delta\rho$ is affected by satellite orbit and it can be written as E.q. (2) by the second raw of cosines.

$$(\rho + \delta\rho)^2 = \rho^2 + B^2 - 2\rho B \sin(\theta - \alpha) \quad (2)$$

Where B is the baseline, θ is the look angle and α is the angle between the horizontal baseline B_H and original baseline B . And $\delta\rho$ is much smaller than ρ , thus E.q. (2) can be rewritten as E.q. (3).

$$\delta\rho \approx -B \sin(\theta - \alpha) + \frac{B^2}{2\rho} \quad (3)$$

And applying E.q. (3) to E.q. (1), the phase of the interferogram can be given by E.q. (4).

$$\phi = -\frac{4\pi}{\lambda} B \sin(\theta - \alpha) + \frac{4\pi}{\lambda} \frac{B^2}{2\rho} \quad (4)$$

2.3 Ambiguity height

After removing topographic phase from interferometric phase, topographic fringes are appeared on interferogram and the amount of height for changing one fringe is ambiguity height (h_a). E.q.(4) can be rewritten as E.q.(5) as $B \sin(\theta - \alpha)$ and $B_{||}$ are the same.

$$\phi = -\frac{4\pi}{\lambda} B_{||} + \frac{4\pi}{\lambda} \frac{B^2}{2\rho} \quad (5)$$

If we differentiate E.q. (5), it can be written as E.q. (6)

$$\frac{d\phi}{d\theta} = -\frac{4\pi}{\lambda} \frac{dB_{||}}{d\theta} = -\frac{4\pi}{\lambda} B_{\perp} \quad (6)$$

At the same time, the relationship between look angle(θ) and topographic height(z) is given by the second raw of cosines in E.q. (7).

$$\cos \theta = \frac{\rho^2 + (r_h + h)^2 - (r_z + z)^2}{2\rho(r_z + h)} \quad (7)$$

If we assume the earth is a sphere, $r_z = r_h = r$ is available. Thus E.q. (7) can be rewritten as E.q. (8).

$$\cos \theta = \frac{\rho^2 + (r + h)^2 - (r + z)^2}{2\rho(r + h)} \quad (8)$$

From E.q. (8), the sensitivity of the height to the look angle can be derived as E.q. (9) and (10).

$$\frac{dz}{d\theta} = \frac{\rho \sin \theta (r + h)}{r + z} \quad (9)$$

$$\frac{dz}{d\theta} = \rho \sin \theta \quad (10)$$

As a result, the sensitivity of the height to the phase change can be written as the following E.q. (11) and (12).

$$\frac{dz}{d\phi} = \frac{dz}{d\theta} \frac{d\theta}{d\phi} = -\frac{\lambda}{4\pi} \frac{\rho \sin \theta}{B_{\perp}} \frac{(r+h)}{(r+z)} \quad (11)$$

$$= -\frac{\lambda}{4\pi} \frac{\rho \sin \theta}{B_{\perp}} \quad (12)$$

From E.q.(12), we can define the ambiguity height as E.q. (13).

$$h_a = -\frac{\lambda}{2} \frac{\rho \sin \theta}{B_{\perp}} \phi \quad (13)$$

In E.q. (13), we can measure the displacement of the ground more effectively if the perpendicular baseline is getting shorter.

2.4 Sensitivity analysis

Interferometric phase contains topography and displacement. If the displacement $\Delta\rho$ is occurred during the observation, the total phase is given by E.q. (14).

$$\phi = \frac{-4\pi}{\lambda} [B \sin(\theta - \alpha) + \Delta\rho] \quad (14)$$

From E.q. (14), the sensitivity of the phase to the topographic height can be written as E.q. (15).

$$\frac{d\phi}{dz} = -\frac{4\pi}{\lambda} \frac{B \cos(\theta - \alpha)}{\rho \sin \theta} = -\frac{2\pi}{h_a} \quad (15)$$

Where h_a is the ambiguity height defined in E.q.(13) and the sensitivity of the phase to the displacement is written as E.q. (16).

$$\frac{d\phi}{d\Delta\rho} = -\frac{4\pi}{\lambda} \quad (16)$$

Considering E.q. (15) and (16), h_a is much bigger than λ . As a result, the sensitivity of the phase is much bigger than topography. As a result, the topographic phase can be measured in metric, while the displacement phase shows centimetric measurement.

2.5 Accuracy analysis

After generating the simulated phase from the conventional DEM, we can remove the topographic phase from a

interferogram by the differential interferometry technique. But it still contains the interferogram error and the DEM error. The interferogram error is given by E.q. (17) and (18).

$$L = \frac{A_p}{R_a R_r} \quad (17)$$

$$(\sigma_{\phi})_{InSAR} = \frac{1}{\sqrt{(2L)}} \frac{\sqrt{1-|\rho|^2}}{|\rho|} \quad (18)$$

Where A_p is the multiplying the multi-look with the pixel size, R_a and R_r means the Azimuth and Range direction resolution. And ρ is the mean correlation value of each image.

On the other hand, the vertical direction displacement error from the phase error is derived by Hagberg and others(1995) and given as E.q. (19).

$$\sigma_z = \frac{\lambda}{4\pi} \frac{R \sin \theta}{B_{\perp}} \sigma_{\phi} \quad (19)$$

Where λ is the wave length, R is the slant range of look direction, θ is the incidence angle and B_{\perp} is the critical baseline. Table 2 shows JERS-1 parameters.

Radar parameter	Value
Frequency, GHz	1.274086
Wavelength, m	0.2353
Sampling Frequency, Hz	17076000
Pulse repetition Frequency, Hz	1555.2001953
Pulse length, μ S	35.0
Chirp slope, Hz/s	-0.42757e12
Range bandwidth, MHz	14.964950
Single look range resolution, m	10.016487
Single look range spacing, m	8.77818
Ground range spacing, m	13.8
Single look azimuth resolution, m	~8
Single look azimuth spacing, m	~4.9
Ground azimuth spacing, m	~4.5
Typical range, m	~724,300
Typical look angle, deg	~35.7(33-38)
Typical incidence angle, deg	~39.4
Critical baseline, m	7000

Table 2. Typical values of JERS-1 parameters(Tobita et al. 1998)

And E.q. (19) can be rewritten conversely as E.q. (20).

$$(\sigma_{\phi})_{DEM} = \frac{4\pi}{\lambda} \frac{B_{\perp}}{R \sin \theta} \sigma_z \quad (20)$$

If we assume that there is no correlation between DEM and interferogram, the total error from each phase is written as E.q. (21) by error propagation.

$$(\sigma_\phi)_{def} = \sqrt{(\sigma_\phi)_{InSAR}^2 + (\sigma_\phi)_{DEM}^2} \quad (21)$$

This phase error can be converted into the slant direction range error(Baek, 2006).

$$(\sigma_z)_{def} = \frac{\lambda}{4\pi} (\sigma_\phi)_{def} \quad (22)$$

3. ESTIMATION OF LANDSLIDE IN KANGWONDO AREA

3.1 Study area

In this study, we considered the mountainous belt of Kangwondo, around Gangneung city (N 37°. 30' ~ 38°. 10', E 128°. 05' ~ 129°. 00') and around Taebaek city (N 36°. 55' ~ 37°. 35', E 128°. 25' ~ 129°. 20') for study area. To measure the displacement, we generated six interferograms for each region from JERS-1 satellite images between 1992 and 1998, and acquired simulated phase by a conventional DEM(Figure. 2) from NASA Shuttle Radar Topography Mission (SRTM). In case of Eurasia, it has the 90m resolution and 9m vertical error (Farr et al. 2007). Through differential interferometry, we subtracted the simulated interferogram from original interferogram and finally generated displacement images for estimating landslide of research area. The satellite image area subjected to analysis is shown in Figure 3.

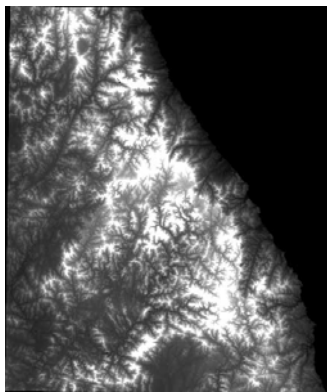


Figure2. The DEM of Kangwon-do area

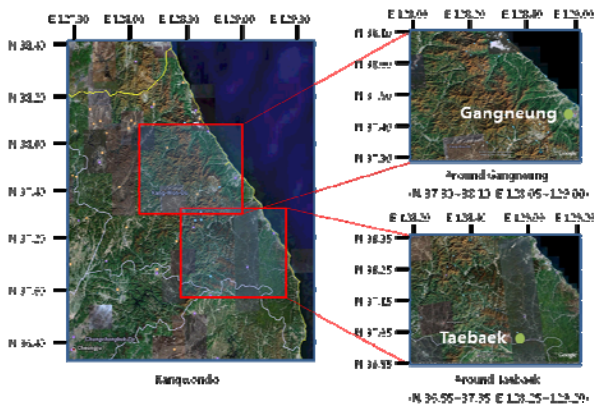


Figure 3. The satellite image of Kangwondo area (Google Earth)

3.2 Generating of interferogram

We need at least two Single Look Complex (SLC) images for interferometry. The before image is specified as the master image and the after image is specified as the slave image. To identify easily, we named each interferogram after their observation date. For example, the interferogram 980705_980818 is generated from master image whose observation date is 1998. 07. 05 and slave image of 1998. 08. 18.

3.3 Baseline

If the two samples are obtained in different time, baseline is determined by the distance between two observations. Theoretically, in case of JERS-1, the critical baseline for interferometry is about 7 km(Baek, 2006). However, long baseline and time interval cause the geometric and temporal decorrelation which can be a factor of phase error. Table 3 shows the baseline of each interferogram in this study.

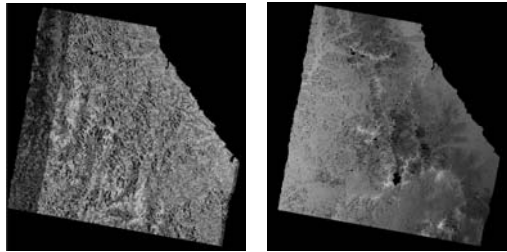
	interferogram	baseline
Gangneung Area	① 930727_930909	375 m
	② 930727_980818	2991 m
	③ 960504_960731	208 m
	④ 960504_980522	269 m
	⑤ 971127_980110	347 m
	⑥ 980705_980818	1675 m
Taebaek Area	① 930908_931022	512 m
	② 931022_980930	3347 m
	③ 960730_961026	145 m
	④ 970830_971013	1722 m
	⑤ 980407_980521	5004 m
	⑥ 980704_980817	1419 m

Table 3. Baseline of repeat pass observation

Consequently, in the case of JERS-1, the baseline is limited less than 1 km for accurate interferometry(Kim et al. 2005). Thus we excluded differential interferogram ②, ⑥ of Gangneung and ②, ④, ⑤, ⑥ of Taebaek from research as their abnormal displacement more than 10m in places. Interferogram ④, ⑤ in Gangneung are also rejected because of its long time interval and expected decorrelation by snow. Thus we only use interferogram ①, ③ in each region.

3.4 Monitoring of landslide around Gangneung city

Figure 4 shows the displacement images generated from differential interferometry. We monitored landslide around Gangneung area from displacement images except for related decorrelation. In the case of 1993, the amount of displacement is measured from -0.742m to 0.958m but the data from 1996 show the measurement from -0.021m to 0.022m, thus we concluded that there was serious landslide during the summer in 1993. Through searching weather forecast record(Figure 5) at that time, we could find that there was a heavy rainfall in 1993. Especially on August 10, a pouring rain more than 220mm in one day was recorded. On the contrary, we had little rain in 1996 comparing with 1993. The precipitation of each month amounts to more or less 200mm and no heavy rain was detected.



① 930727_930909 ③ 960504_960731

Figure 4. The displacement images around Gangneung city

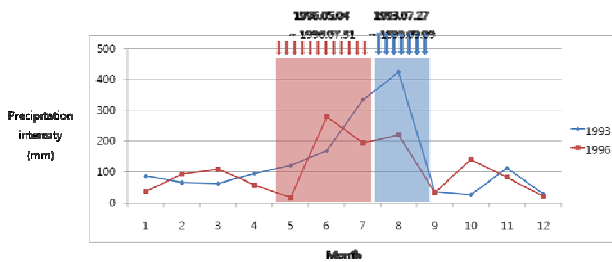


Figure 5. The amount of precipitation in Gangneung city (1993, 1996)

In this study, we used JERS-1 images between 1993 and 1996 but no conventional surveying data available now for comparison because such a long time has passed since then. For accuracy analysis, the error of displacement image was measured $\pm 0.149m$ from E.q. (27). Thus we excluded the image ③ from 1996 for analysis as its displacement was less than error. In the case of image ①, the displacement was measured much higher than the error. Thus, to identify the seriously damaged area by landslide more effectively, we extended the error limit to 0.5m and the result is as showed in Figure 6. The biggest displacement was detected in Audae mountain(N 37°. 5', E 128°. 37') and Gebang mountain(N 37°. 44', E 128°. 29').

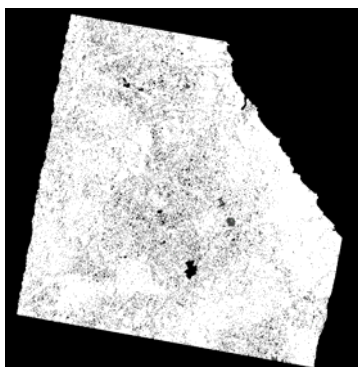
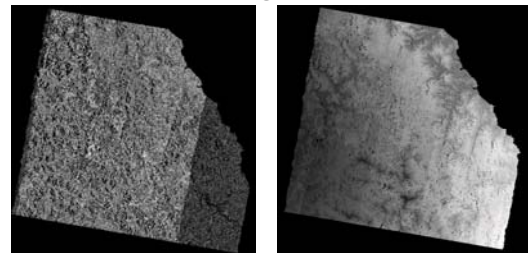


Figure 6. The displacement image around Gangneung city in 1993 (above 0.5m)

3.5 Monitoring of landslide around Taebaek city

Figure 7 shows the displacement images around mountainous belt of Taebaek city in 1993 and 1996. The image ① was generated from 1993 data and ③ was from 1996 data.



① 930908_931022 ③ 960730_961026

Figure 7. The displacement images around Taebaek city

In Korea, we usually have the rainy spell in summer, and the weather forecast record in 1993 and 1996 shows the different precipitation intensity(Figure 8). In the case of 1993, total amount of precipitation was less than 100mm and its displacement was measured only from -0.019m to 0.02m during the season. This result was under the interfergram error 0.149m and no landslide was detected at that time.

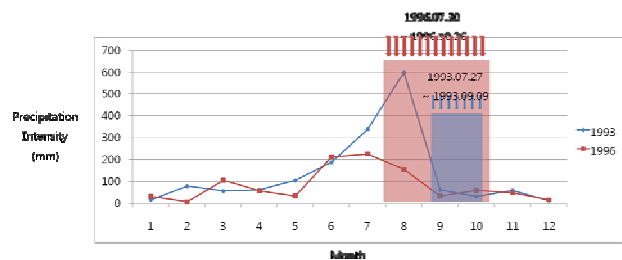


Figure 8. The amount of precipitation in Taebaek city (1993, 1996)

However, some serious displacements were detected in the image ③. Jungsun is located at the center(N 37°. 22', E 128°. 39') and the damaged area were observed on either side, around PyoungChang(N 37°. 25', E 128°. 32'), Yeongweol(N 37°. 13', E 129°. 10'), Nogok(N 37°. 13', E 129°. 10'). Even more than 2m displacement were detected in the west mountainous belt of Uljin(N 37°. 00', E 129°. 08') and the south part of Gagok(N 37°. 08', E 129°. 12'). To identify the seriously damaged places, we set the limit of error to 2m and Figure 9 shows this result.

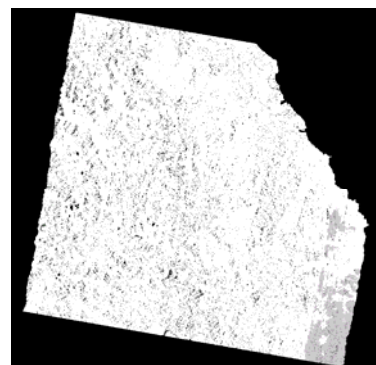


Figure 9. The displacement image around Taebaek city in 1996 (above 2m)

4. CONCLUSION

In this study, through 2-pass differential interferometry technique, we generated displacement image covering Kangwondo and monitor the damaged area by landslide. The important advantage of SAR observation is accurate displacement measuring for broad area. Even if we make allowance for decorrelation by forest, it doesn't cause a serious error in case of L-band sensor as its permeability. We generated 12 interferograms from JERS-1 data and monitored damaged areas by landslide. As a result, Auda and Gebang around Gangneung city, and the west mountainous belt of Uljin and the south part of Gagok around Taebaek city were determined as damaged area by landslide.

Comparing with weather forecast record, the amount of displacement is increased in proportion to the amount of precipitation. This result shows that it is important to detect and cope with the landslide during the rainy spell in summer. Also, the amount of displacement around Taebaek city is measured much bigger than Gangneung city and we consider this is due to its ground condition.

REFERENCES

Achim, H., 2004, *Processing of sar data : fundamentals, signal processing, interferometry*, New York, pp. 1-3.

Baek, S. H., 2006, *DEM Generation and ocean tide modeling over Sulzberger Ice Shelf, West Antarctica, using synthetic aperture radar interferometry*, Ph.D. Dissertation, The Ohio State University, America.

Farr, T. G., Rosen P. A., Caro, E., Crippen, R., Duren, R., Hensley, S., Kobrick, M., Paller, M., Rodriguez, E., Roth, L., Seal, D., Shaffer, S., Shimada, J., Umland, J., Werner, M., Oskin, M., Burbank, D., Alsdorf, D., 2007, The shuttle radar topography mission, AGU.

Hagberg, J. O., Ulander, L. M. H. and Askne, J., 1995. Repeat-pass SAR interferometry over forested terrain, *IEEE Trans. Geosci. Remote Sensing*, 33, pp. 331-340.

Kim, S. W., 2004, *Measurement of surface displacement of Mt. Baekdu and Busan area using L-band SAR interferometry*. Ph.D. Dissertation, The Yonsei University, Korea.

Kim, S. W., Kim, C. O., Won, J. S. and Kim, J. W., 2005, Measurement of ground subsidence in Mokpo area from radar interferometry, *Econ. Environ. Geol.*, 38(4), pp. 381-394.

Massonnet, D., Rossi, M., Carmona, C., Adragna, F., Peltzer, G., Fiegl, K., and Rabaute, T., 1993, The displacement field of the Landers Earthquake mapped by radar interferometry, *Nature*, 364, pp. 138-142.

Rosen, P. A., Hensley, S., Joughin, I. R., Li, F. K., Madsen, S. N., Rodriguez, E., Goldstein, R. M., 2000, Synthetic Aperture Radar Interferometry, *Proceedings of the IEEE*, 88(3)

Tobita, M., Fujiwara, S., Ozawa, S., Rosen, P. A., Fielding, E. J., Werner, C. L., Murakami, M., Nakagawa, H., Nitta, K. and

Murakami, M., 1998, Deformation of the 1995 North Sakhalin earthquake detected by JERS-1/SAR interferometry, *Earth Planets Space*, 50, pp. 313-325.